Final Report

VITROCISET BELGIUM SRL
Rue Devant Les Hetres 2, B-6890 Transinne
Tel+32 61 23.00.04 Fax +32 61 23.02.69
www.vitrocisetbelgium.com
info@vitrocisetbelgium.com
Banque Cbc: 732-0187346-90 Tva: Be 0807.169.365

TELESPAZIO
a LEONARDO and THALES company

VTCB-BE-O3P-RPT-00012, issue 1.0, 30/04/2021

AnREO

Retrieval of total ozone using OLCI/S-3 over Antarctica

Final Report

Funded by

esa

European Space Agency

Authors: A. Kokhanovsky, F. Iodice, A. Zschaege

Approved by: N. De Quattro

Digitally signed by Nicola De Quattro
Date: 2021.04.30 10:22:20 +02'00'

Authorized by: M. Guillaro

Digitally signed by Massimiliano Guillaro
DN: cn=Massimiliano Guillaro
gn=Massimiliano Guillaro c=BE Belgium
l=BE Belgium o=Vitrociset Belgium
ou=Programme and Contract Administration
e=m.guillaro@vitrocisetbelgium.com
Reason: I am the author of this document
Location:
Date: 2021-05-03 11:54+02:00

In this work Vitrociset Belgium has developed a novel algorithm for the total ozone retrieval from spectral top-of-atmosphere solar backscattered light measurements in the spectral range 400-1020nm performed by the ESA Ocean and Land Colour Instrument on board Sentinel-3A/B. The algorithm can be applied for scenes over bright underlying surfaces including clouds, deserts, snow and ice (e.g., over Antarctica), where the ozone absorption feature in the Chappuis absorption band is clearly seen in registered top-of-atmosphere backscattered solar light spectra. The technique provides the possibility to perform the total ozone measurements on the spatial scale 300m, which cannot be reached by other modern spaceborne measurements, aimed at total ozone observations such as TROPOMI, OMI, GOME-2, OMPS and other. The retrieval of TOC using OLCI (0.3km spatial resolution) has been compared with ground measurements (SAOZ, Dobson, Brewer) and multiple satellite TOC measurements (OMI, TROPOMI, OMPS, GOME-2) and ECMWF TOC re-analysis. The comparisons have been shown that the accuracy of OLCI TOC retrieved over snow and ice is comparable with that performed by other satellite missions.

INDEX

Table of Contents

Table of Figures

Table of Tables

Document Change Log

Issue	Date	Changes
1.0	30/04/2021	First issue

1 Introduction

The most of atmospheric ozone (about 90%) is concentrated in the stratosphere, from approximately 15 to 35 km above Earth, although its thickness varies seasonally and geographically. The stratospheric ozone layer absorbs 97 to 99 percent of the Sun´s medium frequency ultraviolet light (from about 200 to 315nm), which otherwise would potentially damage exposed life forms near the surface. The photochemical mechanisms that give rise to the ozone layer are well known. Ozone in the Earth´s stratosphere is created by ultraviolet light striking oxygen molecules containing two oxygen atoms, splitting them into individual oxygen atoms. The atomic oxygen combines with unbroken oxygen molecules (O_2) to create ozone (O_3). The ozone molecule splits into O_2 and an individual atom of oxygen, a continuing process called the ozone – oxygen cycle. Various ozone-depleting substances can be produced at the surface and transported into the stratosphere by turbulent mixing. They release atoms from halogen group through photodissociation, which catalyze the breakdown of ozone into oxygen. From 1987, the production of ozone-depleting substances is not permitted. This stabilized the ozone levels (Montzka et al., 1996, 1999). In particular, the ozone hole over Antarctica (the region, where the total ozone column (TOC) is smaller than 220DU) was the smallest in 2019 ever since it was first discovered about 40 years ago. It is expected that the ozone hole reaches pre – 1980 levels by around 2050 although the 2020 ozone hole (peaked in October) was one of the deepest and largest in recent years covering about 25 million square kilometers.

The total ozone column (TOC) N is defined as follows:

$$N = \int_{h_0}^{h} n(z)dz, \qquad (1)$$

where $n(z)$ is the ozone concentration ($\mathrm{molecules/cm^3}$), h_0 is the altitude of the surface at a given location and h is the top of atmosphere position. Although the integration in Eq.(1) extends over the range of 100 km, the main contribution (90%) to the integral comes from relatively thin ozone layer positioned in stratosphere (usually in the region 15 – 35 km above surface with some variation depending on atmospheric dynamics, temperature, atmospheric chemistry, location and time). The direct method to derive total ozone is the use of balloons (ozonesondes). The balloon ascends to altitudes of about 35 km before it bursts. The heart of the ozonesonde is an electrochemical concentration cell that senses ozone as is reacts with a dilute solution of potassium iodide to produce a weak electrical current proportional to the ozone concentration of the sampled air. As the balloon carrying the instrument package ascends through the atmosphere, the ozonesonde telemeters to a ground receiving station information on ozone concentration at a given position, which can be used to derive total ozone specified in Eq. (1). The data above 35km (1% or so contribution) are extrapolated using the ozone climatology. Although the data of ozonesondes are very accurate and provide useful information at a given location, they area rarely used in practice because they are comparatively expensive and require the presence of personal to operate them.

Usually the measurements of transmitted/reflected solar light spectra in the spectral ranges, where there is strong absorption by ozone, are used for ozone monitoring. The transmitted (direct or diffuse) solar light is analysed by ground - based ozonometers (Dobson, Brewer, and other) and their networks. The determination of the total ozone with spaceborne optical instrumentation is based on the analysis of the solar light reflected by the terrestrial atmosphere.

In this work, funded by the European Space Agency (contracts 4000125043 and 4000130292 – ESA/AO/1-9101/17/I-NB EO Science for Society Permanently Open Call, https://eo4society.esa.int/projects/olci-ozone/) we have developed the novel Total Ozone Retrieval apprOach (TORO). It is based on the spectral top-of-atmosphere solar backscattered light measurements in the spectral range 400-1020nm performed by the ESA Ocean and Land Colour Instrument on board Sentinel -3A, B. The algorithm can be applied for scenes over bright underlying surfaces including clouds, snow and ice (e.g., over Antarctica), where the ozone absorption feature in the Chappuis absorption band is clearly seen in registered top-of-atmosphere backscattered light spectra. The technique provides the possibility to perform the total ozone measurements on the spatial scale 300m, which cannot be reached by other modern spaceborne measurements, aimed at total ozone observations such as TROPOMI, OMI, GOME-2, OMPS and other.

The algorithm is fast and robust. It can be used to study the intra-pixel ozone variability, the study of rapid ozone change across the boundaries of ozone holes and improve ozone retrievals for cloudy areas with a potential looking between clouds. The algorithm can be applied to many optical imagers orbiting the planet and does require high spectral resolution measurements. Also because the algorithm is based on the measurements in the Chappuis absorption band, its sensitivity to the atmospheric pressure and temperature profiles is weak and can be ignored. This makes retrievals simpler. Currently, OLCI retrieval schemes are heavily relied upon ECMWF ozone data supplied in OLCI files. They can be substituted by the results derived from OLCI data itself as shown in this work.

The algorithm can be applied over bright underlying surfaces such as snow, ice, clouds, and deserts. The error of retrievals increases for darker underlying surfaces.

2 Ozone monitoring

Due to importance of stratospheric ozone load in the stratosphere for the survival of life on our planet, the TOC is constantly monitored using ground, balloon, airborne and spaceborne instrumentation. The total ozone determination is based on the measurements of the atmospheric reflectance/transmittance functions in the ozone absorption bands. The main idea behind retrievals is a straightforward one. Namely, both atmospheric transmittance and reflectance functions are characterized by smaller values in the ozone absorption bands as compared to the idealized case, where there is no ozone in atmosphere. The decrease as seen in reflected/transmitted light can be related to the total ozone column (with deeper observed ozone absorption bands for larger total ozone columns). The ozone absorption spectrum in the region 200-1100nm consists of four absorption bands (Hartley (200-330nm), Huggins (320-360nm), Chappuis (400-650nm), and Wulf (above 700nm)). The ground optical instrumentation for the determination of total ozone column often employs the direct solar light measurements in Hartley absorption bands. For instance, the measurements at 305 and 325 nm are used to derive TOC using a network of Dobson spectrophotometers. The measurements in the Huggins bands are most frequently used in spaceborne optical instrumentation. In particular, TROPOMI (on board Sentinel 5p) TOC is derived using the fit of measured and calculated top-of-atmosphere spectral reflectance in the range 325 - 335nm (Spurr et al., 2020). The Chappuis absorption band is also used for the TOC determination both in ground (Pommereau and Gouital, 1988; Sarkissian et al., 1997) and satellite nadir (Jolivet et al., 2016; Kokhanovsky et al., 2020) observations. Fang et al. (2021) has used the limb measurements in the Chappuis – Wulff bands for the ozone profile retrieval (Fang et al., 2021).

The aim of this Project is to modify approach for the TOC determination using the spectral top-of-atmosphere (TOA) measurements over bright surfaces common in Antarctica proposed by Kokhanovsky et al. (2020). In particular, in addition to the radiative transfer modeling, we propose to use the polynomial fit for the determination of the TOA reflectance for an idealized case of ozone absence in atmosphere. Such an approach is common for many satellite total ozone observation techniques (see, e.g., Bouvet, 2012; Jolivet et al. 2016) and is of importance when the underlying surface and atmosphere contain scattering elements, which are difficult to model in the framework of the radiative transfer theory (say, 3-D effects and inhomogeneous underlying surfaces).

The new technique developed by us makes it possible to retrieve the total ozone using high spatial resolution OLCI measurements (300m) and study the rapid changes of TOC in the vicinity of ozone hole boundaries, which is an important addition to other satellite TOC products. We also provide 0.5 degree and 1.0 degree – averaged daily L3 OLCI total ozone product.

3 AnREO Scientific Results

The measured reflectance *R* of solar light from the terrestrial atmosphere in the ozone absorption band can be presented in the following form:

$$R = TR_0, \quad (2)$$

where *T* is the gaseous transmittance in the ozone absorption band and R_0 is the reflectance of atmosphere in absence of ozone in atmosphere. Clearly, in absence of ozone it follows: T=1 and $R = R_0$. In presence of ozone, the transmittance T can be presented as

$$T = \exp(-A\tau), \quad (3)$$

where A is the air mass factor (Iqbal, 1983; Rozanov and Rozanov, 2010) and τ is the ozone vertical optical density defined as:

$$\tau = \int_{h_0}^{h} C_{abs}(z)n(z)dz, \quad (4)$$

where $C_{abs}(z)$ is the ozone absorption cross section at a given altitude *z* and the wavelength λ. Generally, the ozone absorption cross section depends on temperature and pressure and, therefore, on the altitude z in the terrestrial atmosphere. However, this dependence is very weak in the ozone Chappuis absorption band centered at 620nm (Gorshelev et al., 2014) and, therefore, can be ignored. This means that it holds approximately:

$$\tau = NC_{abs} \quad (5)$$

in the Chappius absorption band. This means that the total ozone can be derived directly from the solar light reflectance measurements at a single wavelength (620nm) with the use of the following analytical equation:

$$N = \frac{\ln\left[\frac{R_0}{R}\right]}{AC_{abs}}. \quad (6)$$

Because the value of C_{abs} at 620nm is known from laboratory measurements (3.9806$\times 10^{-21} \frac{cm^2}{molecule}$ (at 194K) or $2.687 \times 10^{16} DU^{-1}$) (see, for example, Gorshelev et al., 2014), the problem of the total ozone retrieval is reduced to the determination of the air mass factor *A* and the value of R_0. The airmass factor depends on many factors including presence of various aerosol species, molecular scattering, observation geometry, the position of the stratospheric layer, etc. (Iqbal, 1983; Rozanov and Rozanov, 2010). Because we are interested in the ozone retrievals over Antarctica, where the aerosol load is low (Six et al., 2005) and we use the wavelength 620nm, where the molecular optical thickness is also low (Tomasi and Petkov, 2015), it is assumed that the Rayleigh scattering air mass factor can be modelled using the following simple analytical equation (Iqbal, 1983; Savastiouk and Mcerloy, 2004):

$$A = \frac{1+s}{\sqrt{2s+\mu_0^2}} + \frac{1+s}{\sqrt{2s+\mu^2}}, \quad (7)$$

where $s = h/r$, h is the height of the ozone layer, r is the radius of the Earth, μ is cosine of the viewing zenith angle (VZA) and μ_0 is cosine of the solar zenith angle (SZA). We shall assume that (Savastiouk and Mcerloy, 2004) $h = 26 - 0.1L$, where L is the latitude in degrees (the negative number in the southern hemisphere) and *h* is the height of the ozone layer in km. Therefore, it is assumed that *h*=17km exactly over the South Pole. Eq. (7) coincides with the geometric airmass factor at *s=0*.

The reflectance R_0 at 620nm in absence of ozone can be found interpolating OLCI measurements not affected by ozone. In particular, we assume that the dependence $R_0(\lambda)$ can be modelled by the polynomial of the second order in the spectral range 400-865nm with the coefficients derived at OLCI measurements positioned at 400, 753.8, and 865nm (see Fig.1). Such an approach is robust and does not require the modelling of optical signals detected at a satellite (Efremenko and Kokhanovsky, 2021) for the case of underlying complex terrain including rocks, partially snow - covered underlying snow surfaces, glacier dark ice, 'wind glaze' regions, etc. In the case of underlying homogeneous snow surfaces the radiative transfer modelling of atmosphere – underlying snow system is used to derive the value of R_0 at 620nm (Kokhanovsky et al., 2021). The selection between two modes of the R_0 retrieval is performed automatically depending on the value of OLCI reflectances at 761.25nm (oxygen absorption band) and 1020nm (ice absorption band). In particular, the polynomial fit is performed if *R* (761.25nm) is larger than 0.17 and *R*(1020nm) is larger than 0.7. These empirical threshold values (THV) have been determined empirically using large amount of OLCI data over various regions of Antarctica.

This project is aimed at retrievals for the case of cloudless sky and bright underlying surfaces. Therefore, the results are not provided for the cases specified in next table.

Table 3-1 The conditions for OLCI reflectances at which retrievals are not attempted.

N	Parameter	THV	Comment
1	R(400nm)	<0.2	Dark underlying surfaces do not provide needed contrast for the application of the underlying technique
2	R(761.25nm)	>0.3	High values of R(761.25nm) mean cloud contamination. This is due to the fact that clouds screen tropospheric oxygen leading to smaller oxygen vertical depths (larger reflectance) in the oxygen A-band. The THV has been found by manual inspection of oxygen A-band reflectance for cloudy scenes over snow.
3	R(1020nm)	>0.9	High values of R(1020nm) mean too small radii of crystals (cloud contamination). The THV has been found by manual inspection of OLCI data at 1020nm for cloudy scenes over snow.

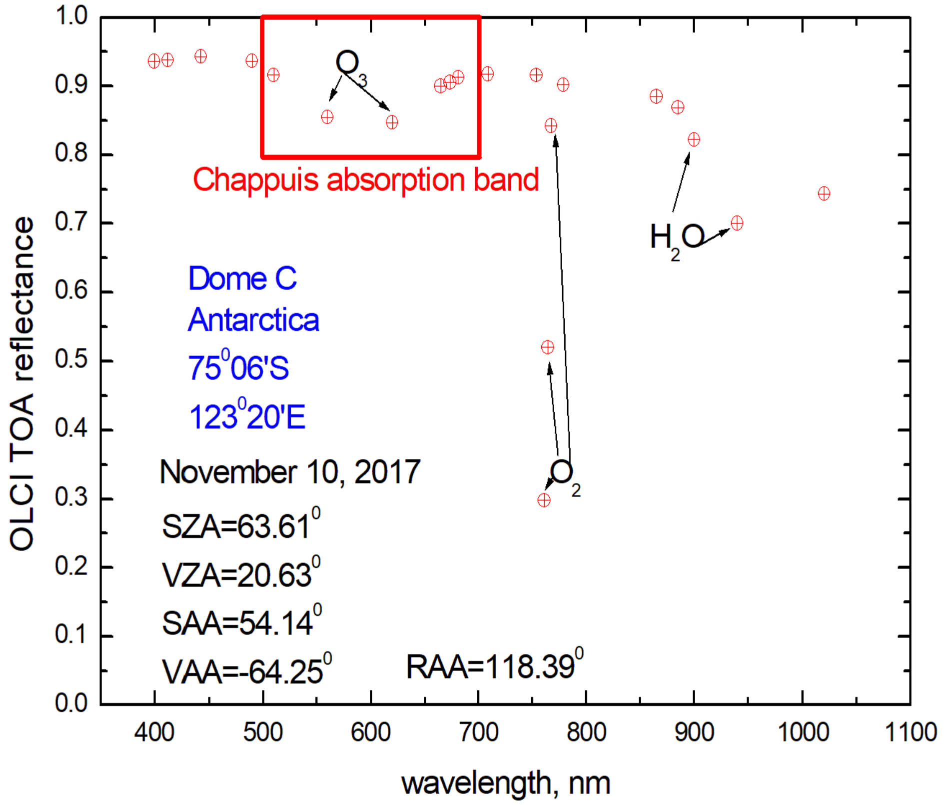

Figure 3-1 OLCI TOA spectrum over snow

Data at solar zenith angle (SZA) equal to 63.61 degrees, viewing zenith angle (VZA) equal to 20.63 degrees, solar azimuthal angle (SAA) 54.14 degrees, and viewing azimuthal angle (VAA) of -64.25 degrees. The relative azimuthal angle is equal to 118.39 degrees. The OLCI measurements have been performed over Dome C (Antarctica) on November 10, 2017. The regions affected by various atmospheric gases are shown.

4 Validity of AnREO Results

4.1 Intercomparison with TROPOMI native resolution measurements

TROPOMI (TROPOspheric Monitoring Instrument)/Sentinel 5p is a spectrometer sensing ultraviolet (UV), visible (VIS), near (NIR) and short-wavelength infrared (SWIR) to monitor ozone, methane, formaldehyde, aerosol, CO, NO_2 and SO_2 in the atmosphere. The TROPOMI total ozone product is derived on the spatial scale 5.5$\times 3.5km^2$ (across$\times$ along track, since August 2019 (5.5$\times 7.5km^2$ at the start of the mission 13.10.2017)) (Spurr et al., 2020). The mean bias and the mean standard deviation between TROPOMI and ground-based TOC is 0-1.5% and 2.5%-4.5% (Garane et al., 2019).

There are two algorithms that deliver TROPOMI total ozone column amounts. The first algorithm (S5P_TO3_DOAS) is based on the "DOAS-style" GOME Data Processor (GDP) algorithm Version 4.8. The second (S5P_TO3_GODFIT) is based on the direct-fitting algorithm developed at BIRA-IASB and used for generating the total ozone Essential Climate Variable as part of the Ozone Climate Change Initiative activities. S5P_TO3_DOAS is used for generation of near-real-time products, while S5P_TO3_GODFIT generates the off-line and reprocessed products. Both algorithms are based on ozone absorption in the UV Huggins bands (325-335 nm). We use exclusively S5P_TO3_GODFIT TOC (Lerot et al., 2010, 2014; van Roozendael et al., 2012) in this work. In particular, L3 0.5 degrees data are derived by the aggregation of TOC derived by the S5P_TO3_GODFIT algorithm on the 5.5$\times 3.5km^2$ spatial resolution scale.

The spatial distribution of TOC derived using S5P_TO3_GODFIT algorithm and that developed by us for OLCI (TORO) is presented in Fig. 2 for spatially and temporally collocated TROPOMI and OLCI pixels. It follows that TORO produces results similar to those provided by TROPOMI S5P_TO3_GODFIT TOC algorithm.

The difference of OLCI and TROPOMI TOCs averaged over the scene is -5.3% (-14.3DU) (see Figure 4-2 and Figure 4-3) with OLCI TOCs on average smaller as compared to TROPOMI TOCs. The average TOC for the scene is 258 DU for OLCI as compared to 272 DU for OMI. The difference arises mostly from the areas, where there is a large gradient in total ozone (and also enhanced total ozone dynamics) with not negligible changes of TOC on the scale of TROPOMI pixel. Note that the total ozone is assumed to be constant for the whole pixel in the TROPOMI ozone retrieval technique (even if it is not the case as it is at the ozone hole boundaries). The case presented in next figure is characterized by the presence of ozone hole boundary (blue color) with strong temporal/spatial variations. Therefore, one may expect differences between measurements performed by both instruments due to temporal mismatch of measurements and uncertainties related to the total ozone retrievals at the ozone hole boundaries.

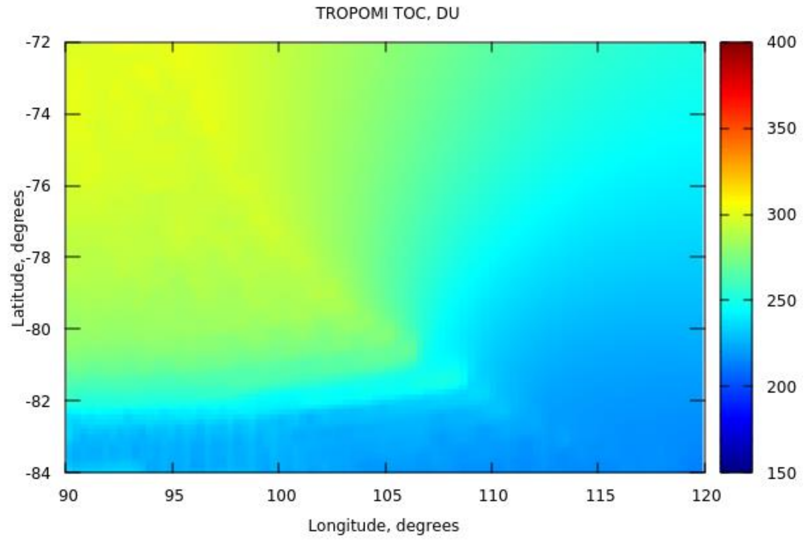

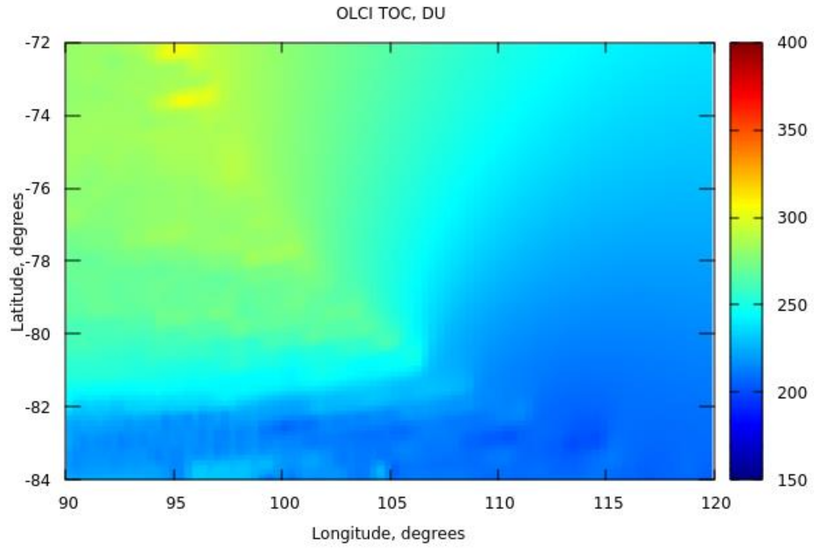

Figure 4-1 The spatial distribution of ozone

Spatial distribution of ozone as derived from TROPOMI and OLCI measurements on December 23, 20:00 (UTC). The OLCI TOCs are averaged on the scale of TROPOMI pixel. The maximal temporal mismatch is 5min.

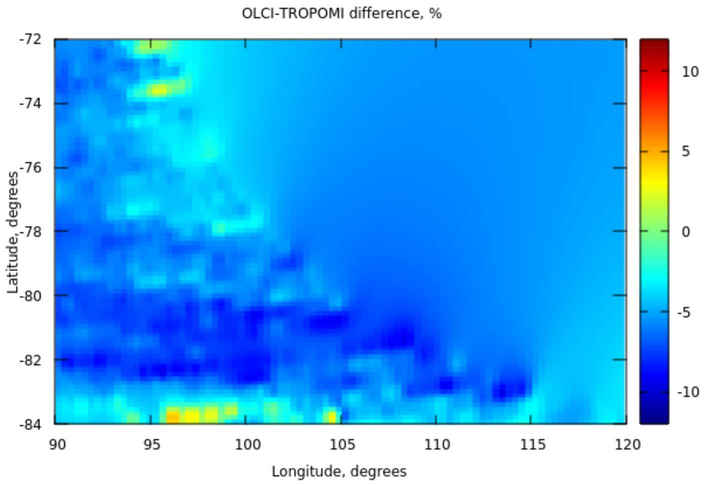

Figure 4-2 The spatial distribution of relative difference between OLCI and TROPOMI total ozone products

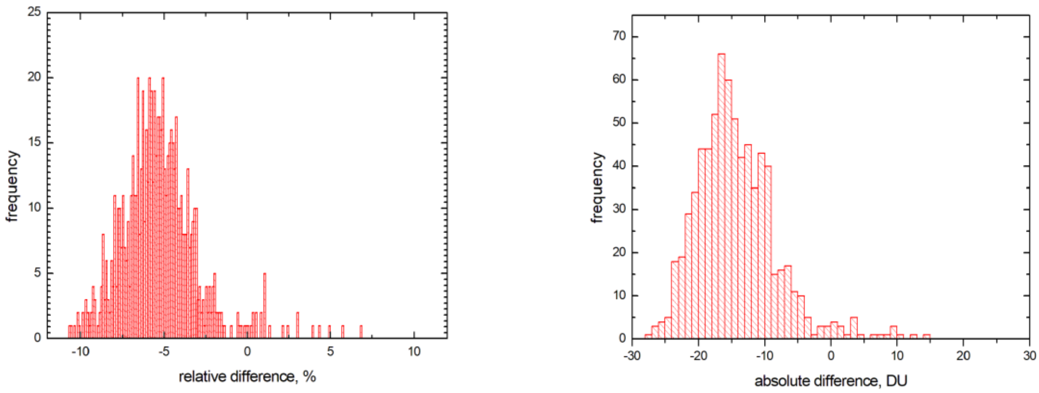

Figure 4-3 The statistical distributions of relative and absolute differences of TOC derived from OLCI and TROPOMI for the case studied.

The difference of OLCI and TROPOMI daily 1 degree-gridded TOC for January 16, 2020 is presented in Figure 4-4. There is no ozone hole in the area studied and the spatial distribution of TOC is relatively smooth. The spatial distribution of the relative difference of both products is shown in Figure 4-5. The statistical distribution of relative and absolute differences are given in Figure 4-6. It follows that TROPOMI and OLCI datasets give very similar TOC spatial distributions with almost no bias (see Figure 4-6).

OLCI TROPOMI

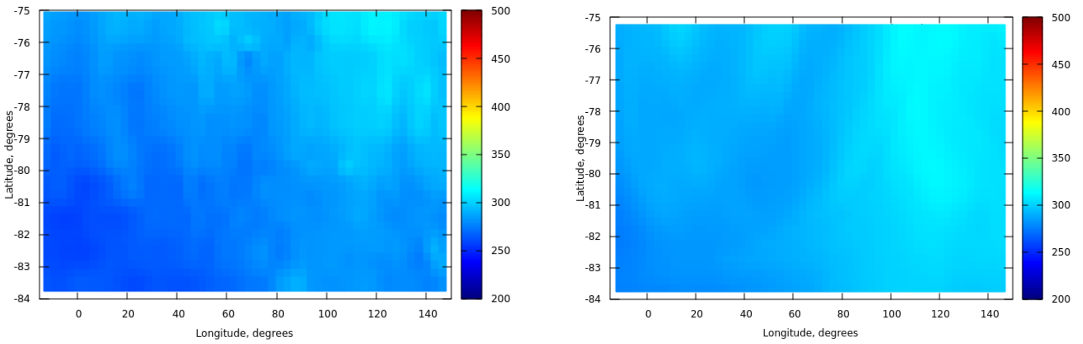

Figure 4-4 The spatial distribution of ozone as derived from TROPOMI and OLCI measurements

The spatial distribution of ozone as derived from TROPOMI and OLCI measurements (1 degree - gridded product) on January 16, 2020. The results averaged for the whole day are presented.

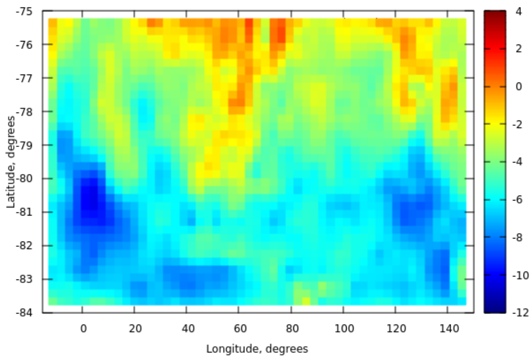

Figure 4-5 The spatial distribution of the difference between OLCI and TROPOMI measurements over Eastern Antarctica

The spatial distribution of the difference between OLCI and TROPOMI measurements over Eastern Antarctica derived from data shown in Figure 4-4

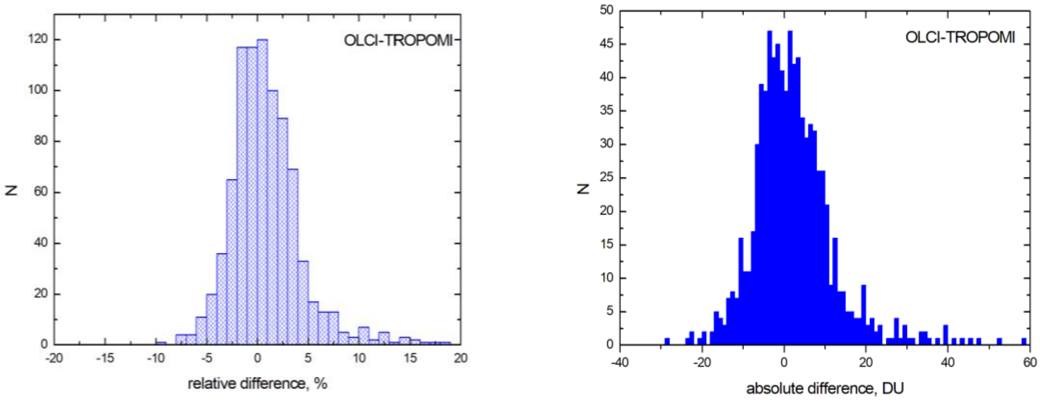

Figure 4-6 The statistical distributions of relative and absolute differences of total ozone column derived from OLCI as compared to TROPOMI

The statistical distributions of relative and absolute differences of total ozone column derived from OLCI as compared to TROPOMI for the case shown in Figure 4-4. The average bias with TROPOMI is 0.8 % (the average standard deviation is 4% and the average absolute difference is 2.2DU).

4.2 Intercomparison with other total ozone products

The total ozone is observed by multiple optical instrumentation. This includes apart of TROPOMI, Ozone Monitoring Instrument (OMI)/AURA, The Ozone Mapping and Profiling Suite (OMPS)/Suomi NPP, Global Ozone Monitoring Experiment -2 (GOME-2)/METOP-A, B, C and some others. The short description of OMI, OMPS, and GOME-2 instruments and respective total ozone retrieval algorithms is given by Kokhanovsky et al (2021). The spatial resolution of these instruments and also their equator crossing time are presented in next table (including OLCI and TROPOMI). We also give a link to the datasets used in this Section (L1 data for OLCI and L3 data for other instruments). The intercomparison of temporal TOC series for November - December 2020 (2020 ozone hole event) for DOME C (Antarctica) is given in Figure 4-7. We interpolated the satellite 1 degree–gridded data (on a fixed grid) to the location of DOME C. It follows that all instruments including OLCI produce similar patterns of ozone temporal variation over DOME C with the ozone hole disappearance on December 13, 2020 and an extreme total ozone variation (100DU) during just 3 days (12-14 December, 2020).

The monthly averaged values (for November, 2020) of TOC derived from various products over DOME C is given in Table 4-2. We also show the monthly averaged values of relative (%) and absolute differences of OLCI TOC from other satellite products in the same Table. The relative/absolute differences of OLCI TOC with that of OMI, OMPS, and TROPOMI is smaller than 1%/2DU. There is a larger deviation to GOME-2 being smaller than 4%/6.4DU.

Table 4-1 The satellite datasets used in this work

Instruments and spatial resolution	Links/algorithms used	Equator crossing time, UTC
OLCI, 0.3x0.3km^2	https://scihub.copernicus.eu/ L1 dataset	10:00
TROPOMI 3.5x5.5km^2	https://s5phub.copernicus.eu/ S5P_TO3_GODFIT	13:30
OMI, 13x24km^2	https://acdisc.gesdisc.eosdis.nasa.gov/opendap/hyrax/HDF-EOS5/Aura_OMI_Level3/OMTO3d.003/ OMTO3d algorithm	13:38
OMPS, 50x50km^2 (Nadir Mapper)	https://disc.gsfc.nasa.gov/datasets/OMPS_NPP_NMTO3_L3_DAILY_2/summary NMTO3 algorithm	13:30
GOME-2, 80x40km^2	http://atmos.caf.dlr.de/gome2 DOAS	9:30

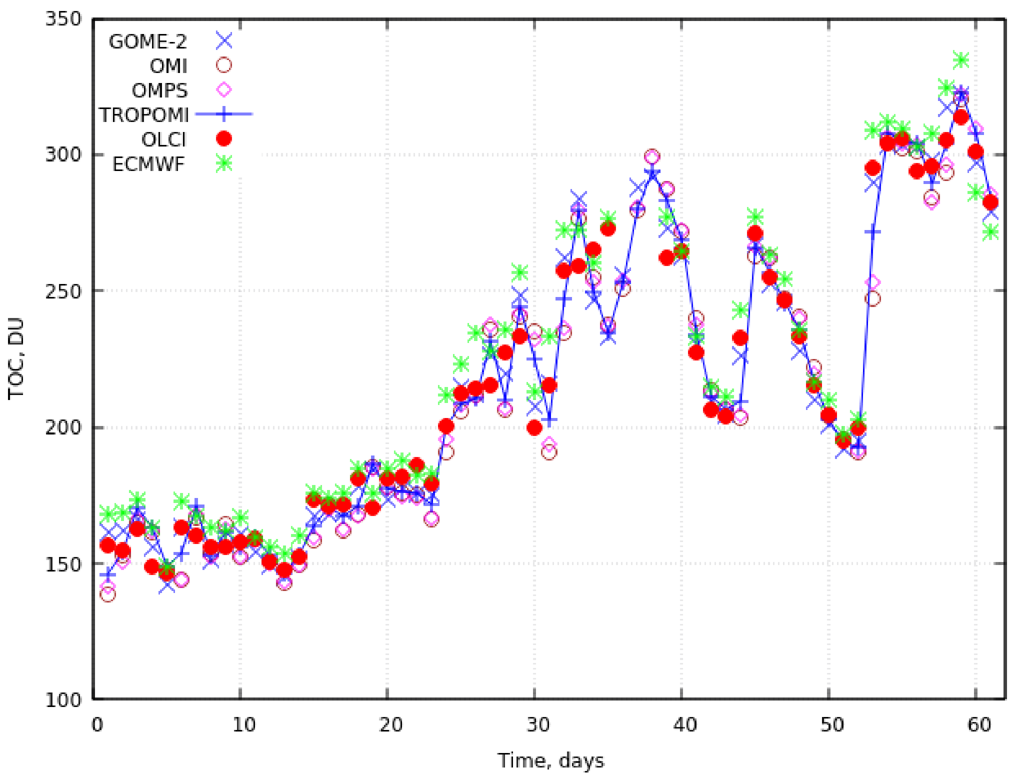

Figure 4-7 The time series of total ozone over Dome C (Antarctica) for November – December 2020

The time series of total ozone over Dome C (Antarctica) for November – December 2020 derived using various optical instrumentation and ECMWF re-analysis. The 1 degree -gridded TOC product over the site has been used.

Table 4-2 The intercomparison of monthly averaged TOCs RD and AD

The intercomparison of monthly averaged TOCs relative differences (RD) and absolute differences (AD) over DOME C (Antarctica) (November, 2020)

Instrument	TROPOMI	OMI	OMPS	GOME-2	OLCI
<TOC>	176	173.9	174	169.3	175.7
RD, %	-0.2	1.0	1.0	3.8	-
AD, DU	-0.4	1.8	1.7	6.4	-

4.3 Intercomparison with ground measurements of total ozone

The direct solar light attenuation measurements are performed by Dobson and Brewer spectrophotometers in Antarctica on a regular basis. The measurements by Dobson spectrophotometers are used to retrieve the total ozone column by comparing two different wavelength intensities, UVB (305 nm) and UVA (325 nm). The technique has its drawbacks. It is strongly affected by aerosols and pollutants in the atmosphere, because they also absorb some of the light at the same wavelengths. The basic measurement principle of Brewer spectrophotometer is the same as the Dobson one except the Brewer directly measures the intensity of light at a number of different ultraviolet wavelengths. The comparison between OLCI observations and Dobson/Brewer ground measurements of total ozone column are presented in next figures for two ground stations with coordinates specified in Table 4-3. For a reference, we also show the total ozone derived from TROPOMI/S-5p (S5P_TO3_GODFIT algorithm).

For TROPOMI, we have used the latest reprocessing version and the orbit aggregation is daily 0.5° latitude and 0.5° longitude. The OLCI TOC has been averaged for all observations at a given day for the specified locations. The closest to the ground station OLCI pixel has been selected (and similar for TROPOMI). We also have used daily products both for Dobson and Brewer.

It follows that the relative differences between satellite and ground measurements are below 5% for most of cases with some deviations related to the influence of clouds and also spatial mismatch and temporal sampling of ground and satellite measurements. The larger variation of OLCI measurements is due to the fact that we did not apply the spatial averaging procedure for OLCI TOC around the station. The monthly average relative differences of TROPOMI and OLCI measurements of TOC from that performed by the ground stations are shown in Table 4-4 OLCI and TROPOMI TOCs are very close for the measurements at Halley. The OLCI TOC is systematically higher as compared to both the TROPOMI and Brewer measurements.

The overview of the differences of OLCI TOC from TOCs provided in other satellite and ground measurements datasets is given in Table 4-5. Overall, we conclude that OLCI provides accurate and robust total ozone product with the relative difference to other datasets over bright surfaces smaller than about 5%. The differences decrease, if daily, monthly or space-averaged date are inter-compared.

The OLCI, OMI and TROPOMI total ozone over the whole Antarctica is presented in Figure 4-10 for January 16, 2020. One can see that all three instruments produce coherent patterns of spatial distribution of total ozone column over Antarctica. The 2020 ozone hole as monitored by both TROPOMI and OLCI is presented in Figure 4-11 for December 20, 2020 just one week before its disappearance. We can see that both instruments produce very similar spatial distributions of total ozone over Antarctica with ozone hole existing over Eastern Antarctica and clear signs of ozone recovery in the Western Antarctica.

Table 4-3 Selected Antarctic ground stations

The coordinates of selected Antarctic ground stations, where the TOC measurements are performed

Station	Country	Latitude/Longitude	Site altitude, m	Instrument
Halley	UK	-75.36/-26.13	33	Dobson, Beck, 73
Zhong Shan	China	-69.37/76.38	11	Brewer, MKIII, 193

a) b)

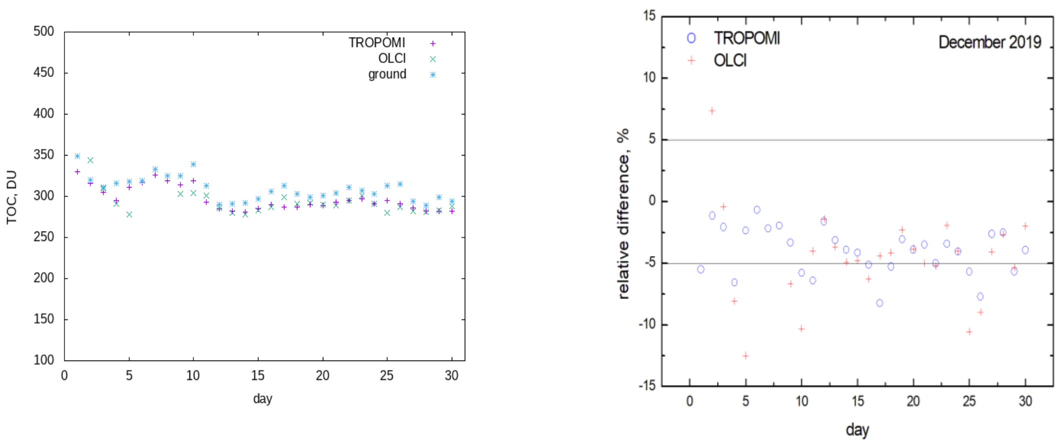

Figure 4-8 Comparison with Halley Station

(a) The time series of TOC derived from OLCI and TROPOMI 0.5 deg averaged daily TOC product and from ground Dobson measurements (also daily product) at the Halley station in December 2019 , (b) The relative differences of satellite and ground measurements. (a) The time series of TOC derived from OLCI and TROPOMI 0.5 deg averaged daily TOC product and from ground Dobson measurements (also daily product) at the Halley station in December 2019 , (b) The relative differences of satellite and ground measurements.

a)

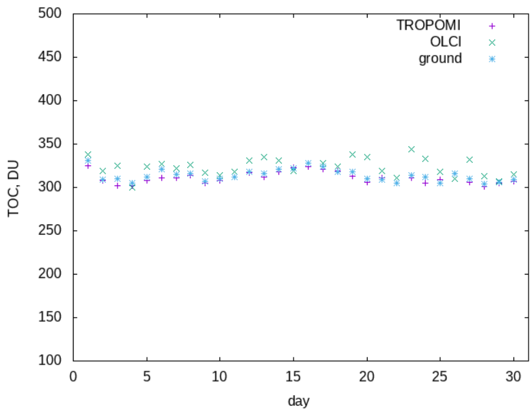

b)

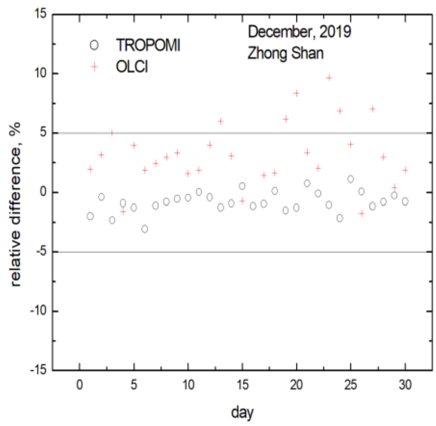

Figure 4-9 Comparison with Antarctic Zhong Shan station

(a) The time series of daily TOC derived from OLCI, TROPOMI and from ground Brewer measurements at the Antarctic Zhong Shan station in December 2019. (b) The relative difference of satellite and ground measurements.

Table 4-4 The monthly - averaged comparison with at Halley and Zhong Shan stations (Antarctica)

The monthly - averaged relative differences (RD) and standard deviations (STDV) of OLCI and TROPOMI TOC satellite measurements from ground measured TOC at Halley and Zhong Shan stations (Antarctica) in December 2019.

Station	RD/STDV (OLCI), %	RD/STDV (TROPOMI), %	Instrument
Halley	-4.6/3.8	-4/2	Dobson, Beck, 73
Zhong Shan	3.2/2.7	-0.8/0.9	Brewer, MKIII, 193

Table 4-5 The intercomparison of OLCI TOC with other TOC products

Dataset	Region	Time	RD, %	AD, DU	Spatial resolution
Collocated in time and space TROPOMI TOC (S5P_TO3_GODFIT algorithm) native spatial resolution measurements (with ozone hole)	72-84S 90-120E	23.12.2020 20:00UTC$\pm$5min	-5.3	-14.3	3.5x5.5km
Collocated in space TROPOMI 0.5 degree - gridded TOC measurements	75-84S 20W-150E	16.01.2020 (daily product)	0.8	2.2	0.5deg

TROPOMI, OMI, OMPS, and GOME-2 1deg -gridded TOC measurements	75.1S, 123.3E (DOME C)	November, 2020 (monthly average)	-0.2/1/1/3.8	-0.4/1.8/1.7/6.4	1.0deg
Dobson (Beck, 73) ground ozone measurements	75.36S, 26.13W (Halley)	December, 2019 (monthly average)	-4.6	-13.4	0.3x0.3km
Brewer (MKIII, 193) ground ozone measurements	69.37S, 76.38E (Zhong Shan)	December, 2019 (monthly average)	3.2	10.0	0.3x0.3km

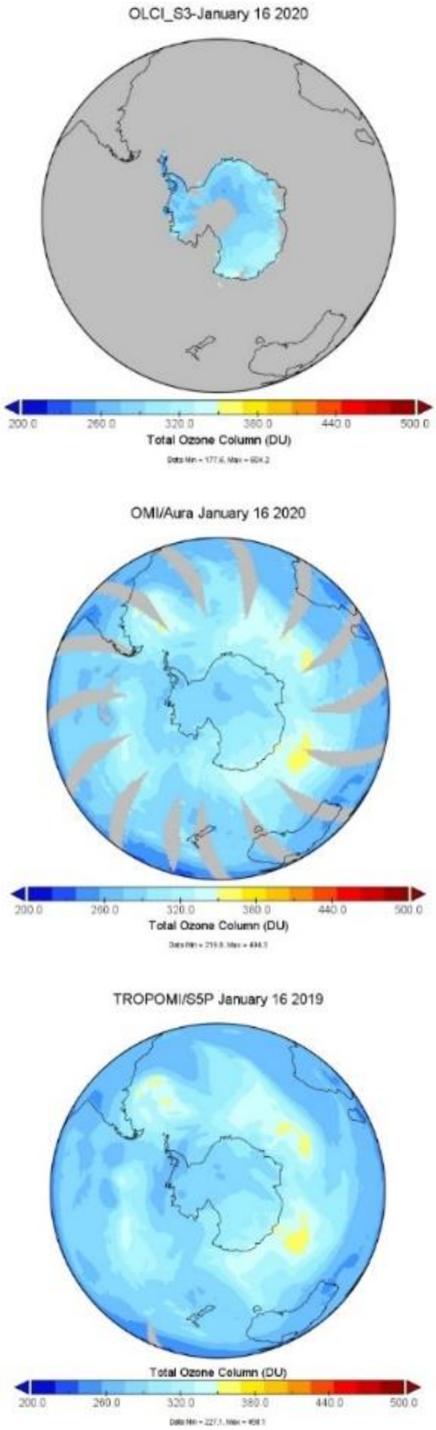

Figure 4-10 OLCI, TROPOMI and OMI comparison

The OLCI, TROPOMI and OMI total ozone columns over Antarctica for January 16, 2020. The southern limit of OLCI measurements is 84.4 degrees south. Therefore, the area close to the South pole is not covered. The OLCI TOC retrievals have not performed over ocean.

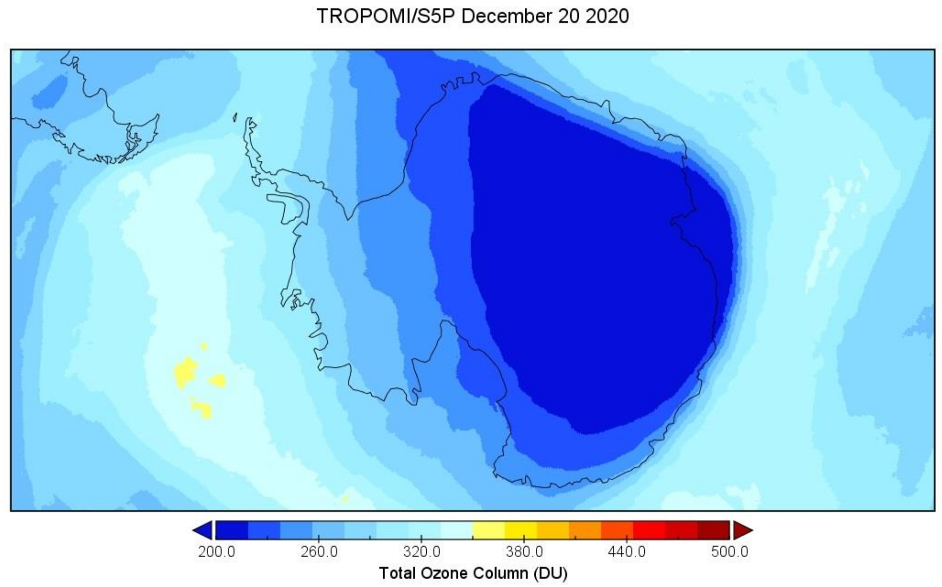

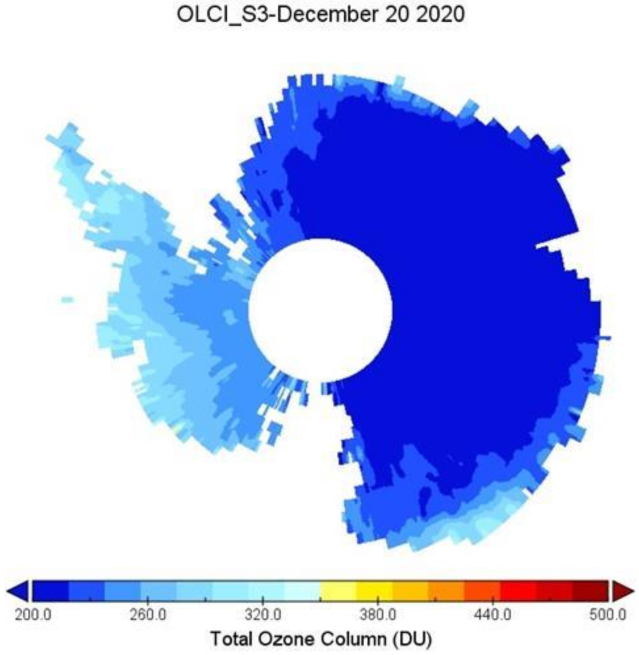

Figure 4-11 The OLCI and TROPOMI total ozone columns over Antarctica.

The OLCI and TROPOMI total ozone columns over Antarctica for December 20, 2020, just a weak before the disappearance of ozone 2020 hole over Antarctica.

5 Conclusions and recommendations

The OLCI total ozone product has been developed. The technique is based on the analysis of the top-of-atmosphere measurements in the Chappuis ozone absorption bands and has the heritage in a similar TOC product developed for Medium Resolution Imager MERIS onboard ENVISAT(Jolivet et al., 2016).

The product can be used for the cases of bright underlying surfaces such as snow and ice for clean sky cases. The average differences from other TOC datasets are below 5%. The OLCI TOC is provided on the 300m spatial resolution and also on the 0.5 and 1.0 degree grid similar to other satellite products. The accuracy of the product increases for larger averaging scales both in space and time domains.

The OLCI TOC product can be used instead of ECMWF total ozone product provided in the OLCI instrument files in the case of measurements over snow and ice surfaces. The algorithm developed here can be also applied to data of OLCI/S-3C,D to be launched in the near future. Therefore, the long- term record total ozone record based exclusively on OLCI measurements can be prepared.

The technique can be applied to a number of current optical instruments performing top-of-atmosphere measurements in the spectral range 400-1000nm with moderate and high spatial resolution. This makes it possible to derive the total ozone with the spatial resolution of 0.3-1km, which is of importance for the understanding intra-pixel TOC ozone variability for the optical instrumentation performing measurements at coarse spatial resolution and also for the enhanced accuracy of retrievals at the areas, where the spatial variability is at maximum (say, at ozone hole boundaries). The technique allows for a simple extension for the total ozone profile determination from limb measurements.

The future development of the algorithm requires its extension to the areas covered by clouds (e.g., in the framework of the ozone ghost column approach) and enhancement of its accuracy for darker areas and also for the cases of inhomogeneous underlying surfaces.

6 References

Bouvet M., *Total column ozone retrieval from MERIS*, version 3.1, 15/11/2012 (available from ftp://ftp.estec.esa.int/pub/xe/anonymous/TN_Ozone_Retrieval_Bouvet_v3.1.pdf).

Efremenko, D., and A. A. Kokhanovsky, 2021: *Foundations of Remote Sensing*, Berlin: Springer.

Garane, K., et al., 2019: TROPOMI/S5P total ozone column data: global ground-based validation and consistency with other satellite missions, *Atmos. Meas. Techniques*, 12, 5263-5287.

Gorshelev, V., Serdyuchenko, A., Weber, M., Chehade, W., and Burrows, J. P., 2014: : High spectral resolution ozone absorption cross-sections – Part 1: Measurements, data analysis and comparison with previous measurements around 293 K, *Atmos. Meas. Tech*., 7, 609–624, https://doi.org/10.5194/amt-7-609-2014.

Iqbal, M., 1983: *An Introduction to Solar Radiation*, New York: Academic Press, p. 101.

Jolivet, D., Bouvet, M., Lerot, C., Van Roozendael, M., Ramon, D. 2016: TORMS: Total ozone retrieval from MERIS in view of application to Sentinel-3, *Proceedings of Living Planet Symposium* 2016, Vol. 740, https://orfeo.kbr.be/handle/internal/4434.

Kokhanovsky, A. A., Lamare, M., Rozanov, V.V., 2020: Retrieval of the total ozone over Antarctica using Sentinel-3 Ocean and Land Colour Instrument, *Journal of Quantitative Spectroscopy and Radiative Transfer*, 251, 107045, https://doi.org/10.1016/j.jqsrt.2020.107045.

Kokhanovsky, A.A., et al., 2021: Retrieval of total ozone column using high spatial resolution top-of-atmosphere measurements by OLCI/S-3 in the ozone Chappuis absorption bands over bright underlying surfaces, *Frontiers in Environmental Science*, in preparation.

Lerot, C., M. van Roozendael, J. van Gent, D. Loyola, and R. Spurr, The GODFIT algorithm: a direct fitting approach to improve the accuracy of total ozone measurements from GOME, Int. J. Remote Sensing, 31(2), 543-550, doi: 10-1080/01431160902893576, 2010.

Montzka, S. A., Butler, J. H., Myers, R. C., Thompson, T. M., Swanson, T. H., Clarke, A. D., ... & Elkins, J. W., 1996: Decline in the tropospheric abundance of halogen from halocarbons: Implications for stratospheric ozone depletion. Science, 272(5266), 1318-1322.

Montzka, S., Butler, J., Elkins, J. et al., 1999: Present and future trends in the atmospheric burden of ozone-depleting halogens. Nature 398, 690–694. https://doi.org/10.1038/19499

Pommereau, J.-P. and Goutail, F.: O3 and NO2 ground-based measurements by visible spectrometry during arctic winter and spring 1988, Geophys. Res. Lett., 15, 891–894, 1988.

Rozanov, V. V. and Rozanov, A. V., 2010: Differential optical absorption spectroscopy (DOAS) and air mass factor concept for a multiply scattering vertically inhomogeneous medium: theoretical consideration, *Atmos. Meas. Tech*., 3, 751–780, https://doi.org/10.5194/amt-3-751-2010, 2010.

Sarkissian A., et al., 1997: Accuracy of measurements of total ozone by a SAOZ ground-based zenith sky visible spectrometer, *J. Geophysical Research*, 102, 1, p.1379-1390.

Savastiouk, V., C. T. McErloy, 2004: Calculating air mass factors for ozone and Rayleigh air mass factor calculations for ground – based spectrometers, Proc. Of Quadrennial Ozone Symposium,Kos, Greece, doi: 10.13140/2.1.3553.7284.

Six D., M. Fily, L. Blarel, P. Goloub, 2005: First aerosol optical thickness measurements at Dome C (east Antarctica), summer season 2003-2004, Atmos. Env., 39, 5041-5050.

Spurr R., D. Loyola, M. Van Roozendael, C. Lerot, K-P. Heuse, and J. Xu, 2020: S5P/TROPOMI total ozone ATBD, S5P-L2_DLR-ATBD-400A.

Tomasi, C., and B. H. Petkov, 2015: Spectral calculations of Rayleigh – scattering optical depth at Arctic and Antarctic sites using a two – term algorithm, *J. Geophys. Res.*, 10.1002/2015JD023575.

Van Roozendael, M., R. Spurr, D. Loyola, C. Lerot, D. Balis, J-C. Lambert, W. Zimmer, J. van Gent, J. van Geffen, M. Koukouli, J. Granville, A. Doicu, C. Fayt, C. Zehner, Sixteen years of GOME/ERS2 total ozone data: the new direct-fitting GOME Data Processor (GDP) Version 5: I. Algorithm Description, J. Geophys. Res., 117, D03305, doi:10.1029/2011JD016471, 2012.

END OF THE DOCUMENT